+ MODEL

Available online at www.sciencedirect.com
SCIENCE DIRECT®

Surface & Coatings Technology xx (2005) xxx – xxx

SURFACE & COATINGS TECHNOLOGY

www.elsevier.com/locate/surfcoat

Mechanical properties of cold-sprayed and thermally sprayed copper coatings

F. Gärtner [a,*], T. Stoltenhoff [a], J. Voyer [a], H. Kreye [a], S. Riekehr [b], M. Koçak [b]

[a] Helmut Schmidt University, Holstenhofweg 85, 22043 Hamburg, Germany
[b] GKSS-Research Center Geesthacht GmbH, Institute for Materials Research, Max-Planck-Straße, 21502 Geesthacht, Germany

Received 17 August 2005; accepted in revised form 11 October 2005

Abstract

The present investigation compares the mechanical properties of cold-sprayed and thermally sprayed copper coatings. The mechanical properties of the Cu-coatings are determined by in plane tensile test using micro-flat tensile specimen technique. A deeper view into the type of obtained defects, their stability and their influence on coating performance, is supplied by subsequent failure analyses and the comparison to annealed copper coatings. The results demonstrate that cold-sprayed coatings, processed with helium as propellant gas, show similar performance as highly deformed bulk copper sheets and respective changes in properties after annealing. In the as-sprayed condition, cold-sprayed coatings processed with nitrogen and thermally sprayed coatings show rather brittle behavior. Whereas subsequent annealing can improve the properties of the cold-sprayed coating, processed with nitrogen, such heat treatments have only minor influence on the tensile properties of thermally sprayed copper coatings. The investigation of failure modes for the as-sprayed states and after different heat treatments provided further information concerning particle–particle bonding and the effect of oxides on mechanical properties.

Keywords: Cold spraying; HVOF spraying; Arc spraying; Mechanical properties

1. Introduction

In thermal spraying, major developments within the last three decades aimed to operate spray systems at lower process temperatures and respectively increased gas and particle velocities [1]. These attempts to shift the balance between thermal and kinetic energies towards the latter were driven by the goal to reduce disadvantageous effects on coating properties like oxidation, phase transformations or crack formation due to stresses introduced during rapid solidification of the spray material on the substrate. In the comparison of currently available spray techniques, cold spraying (CS) just represents a range at the extreme end with process temperatures far below the melting point of respective spray materials and with very high gas and particle velocities [2]. These process characteristics make cold spraying particularly suitable for oxidation-sensitive materials [3,4].

The adhesion of particles in cold-sprayed coatings is solely the result of the high-energy impact of solid particles. As in explosive cladding or explosive powder compaction, bonding can be attributed to the degree of deformation and the associated temperature rise at particle–particle and particle–substrate interfaces [5]. The localized rise in plastic flow by shear instabilities is a necessary requirement for successful bonding. Criteria for bonding are only met if the particles exceed a certain critical impact velocity, which is specific to the coating and the substrate material. For copper powder with a particle sizes distribution from 5 to 22 μm, the critical velocity was determined to range from 530 to 560 m/s [5,6]. The high gas and particle velocities in cold spraying are obtained by the expansion and acceleration of a heated and highly pressurized gas during the flow through a DeLaval-type nozzle. The principle of the technical set-up for cold spraying is described elsewhere [3,4].

For the current study, copper was chosen as spray material with respect to the high deformability, the available variety of powder feedstock with different oxygen contents, a high amount of reference data and interests concerning

* Corresponding author. Tel.: +49 40 6541 2887; fax: +49 40 6541 2006.
E-mail address: frank.gaertner@hsu-hh.de (F. Gärtner).

0257-8972/$ - see front matter © 2005 Elsevier B.V. All rights reserved.
doi:10.1016/j.surfcoat.2005.10.007

applications [7]. To cover a wide range between thermal and kinetic particle impact energy in thermal spraying, arc spraying (AS) and high velocity oxy-fuel flame (HVOF) spraying were chosen as processes, serving as reference [7]. As further reference, respective analyses were also performed for cold rolled, high purity copper (OFHC). A number of defects introduced by thermal or cold spraying, can heal out during annealing. To study their nature and respective consequences on coating properties, subsequent heat treatments were applied to the various copper coatings. Recent investigations already demonstrated that high velocity impacts as obtained in HVOF or cold spraying result in a type of persistent defect in the form of dislocation loops, which enhance hardness and correlate well to the recombination of non-equilibrium vacancies and interstitials observed after heavy ion implantation [8]. The study of coating properties after annealing is also of interest with respect to applications. The first industrial use of cold spraying involves soldering of the coated parts and thus a heat treatment after coating deposition [9].

Recent investigations on the comparison of thermally sprayed and cold-sprayed copper coatings supplied information concerning microstructural details, deposition efficiencies, and properties like bond strength, hardness and electrical conductivity [7]. The present study aims to supply a more detailed view on intrinsic tensile properties of the copper coatings and thus on particle–particle bonding attained in cold spraying in comparison to thermal spraying in as-sprayed and heat-treated states.

Mechanical properties of thermal spray coatings are often investigated by bend tests [10–12] with specimens containing coating and substrate materials together. Such analyses need careful consideration to distinguish influences by the substrate material, the adhesive strength of the coating–substrate interface and the internal stress in the coating. The real performance of the coatings with respect to mechanical properties can only be investigated by direct measurements of the stress–stain curves of the samples, prepared from the coating itself. This can depend on the thickness of the coating layer. For the thin layer of coating, a micro-sized specimen extraction and respectively testing is essential.

For the plasma- and HVOF-sprayed copper, tensile tests in combination of the results obtained by X-ray diffraction have already supplied valuable information on coating performance [13]. Recently, in a similar combination of methods, mechanical properties of cold-sprayed copper coatings, processed with helium, were also reported [14]. In that work, as well as in studies of cold-sprayed aluminum coatings or investigating titanium alloy coatings, comparatively thick coatings were prepared to comply with the sample geometries of EN or ASTM requirements [15,16]. However, building up such thick layers leads to heating of the coatings already during the spray process.

Thus, the present study aims to minimize such thermal effects during the coating process by limiting coating thickness to 5 mm. For determination of the full stress–strain curves of the narrow welds (e.g. laser beam) or interface regions of bi-material systems, the micro-flat tensile testing technique was developed by Kocak et al. [17]. The present investigation has used a similar approach for the evaluation of the mechanical properties of the thin copper coatings by extracting multiple thin specimens to determine the properties of the coating in detail.

After tensile testing, metallographic methods are applied to investigate fractured surfaces to improve the understanding of the bonding processes and intrinsic properties of the coatings. The obtained failure morphologies provided valuable information on the effect of defects, present in the different types of coatings, on respective strengths. As reference, the results are compared to those obtained for similarly deformed and heat-treated bulk copper samples.

2. Methods

2.1. Cold spraying, thermal spraying and annealing

Cold spray and thermal spray experiments were performed under previously optimized standard parameter settings [7], whereas substrate material, form and dimensions, as well as coating thickness were chosen with regard to the further investigations. The whole set of parameters used in cold spraying (CS), high velocity oxy-fuel spraying (HVOF) and arc spraying

Table 1
Spray parameters for the preparation of CS, AS and HVOF coatings

	CS: N_2	CS: He	AS (OSU LD/U(A))	HVOF (DJ 2700)
Feedstock	−25+5 μm, gas-atomized powder	−25+5 μm, gas-atomized powder	1.6 mm wire	Diamalloy 1007, −88+31 μm, gas-atomized powder
Spray distance (mm)	30	30	100–120	250
Traverse speed (m/min)	18.7	18.7	–/–	30
System settings	Propellant gas: N_2; 30 bar, 305 °C (87 N m^3/h) Carrier gas: N_2; 31 bar, 15 °C (8.7 N m^3/h)	Propellant gas: He; 25 bar, 300 °C (144 N m^3/h) Carrier gas: N_2; 26 bar, 15 °C (7.2 N m^3/h)	Voltage: 25 V Current: 70–80 A Propellant gas: compressed air	λ=1:2.59 Ethylene: 5–6.2 N m^3/h Oxygen: 9.8–11.7 N m^3/h Cooling gas: compressed air (19–21 N m^3/h)

CS=cold spraying, AS=arc spraying, HVOF=high velocity oxy-fuel spraying.

(AS) is summarized in Table 1. Samples obtained from the various spray methods were subsequently annealed in vacuum for 1 h at temperatures of 200 °C, 400 °C and 600 °C.

2.2. Mechanical properties

For the quantitative analysis of mechanical properties of the coatings, an in-plane tensile test of miniaturized samples, in previous investigations termed 'micro-flat' tensile specimen [17], was performed (for detailed sizes, see Fig. 1). The 'micro-flat' samples with a thickness of 0.5 mm were cut out by spark erosion parallel and perpendicular to the spray tracks. Although the thermal load of the substrate and coating material in cold spraying is relatively low, temperature gradients in the coatings due to their thickness of up to 5 mm were expected to influence the strength distribution within the thickness of the coating. Therefore, series of 0.5-mm-thick flat tensile specimens were extracted in coating thickness direction towards the substrate (Fig. 1).

For each condition, three samples were tested. Tensile tests were performed on a universal electromechanical test machine and the elongation was measured by an integrated, angular scanner laser extensometer. This type of analysis scans the measuring range with a visible laser beam. To supply sufficient contrast, the samples had to be coated with highly reflecting stripes perpendicular to the deformation direction. The positions of these marks are continuously monitored during the tensile tests.

To evaluate whether the processing of such test samples out of copper influences their performance, comparative experiments using standard flat samples according to EN 10002-1 and 'micro-flat' samples were performed in rolling direction for high purity copper, cold rolled to 70% in reduction of thickness and, for rolled cooper, additionally annealed for 1 h at 350 °C.

2.3. Deformation microstructures, fracture and erosion morphologies

To reveal the deformation within the areas of failure in tensile tests, cross-sections of respective samples were prepared

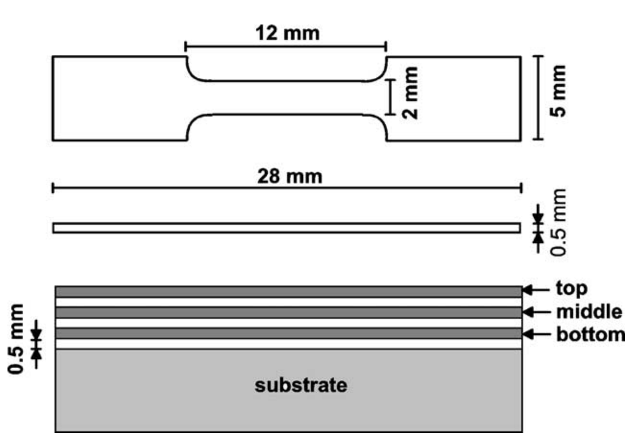

Fig. 1. Dimensions of the micro-flat tensile test samples and their orientation within the coating.

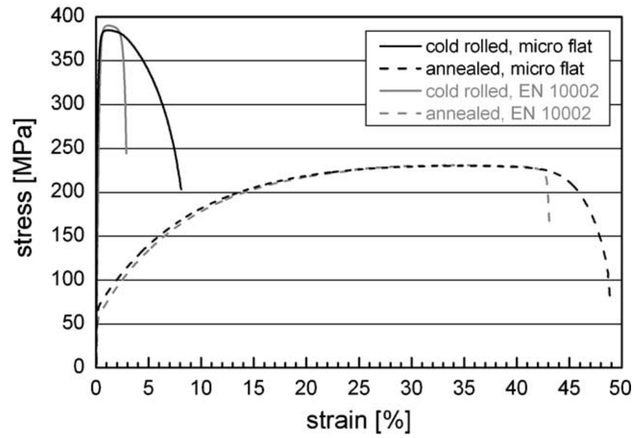

Fig. 2. Comparison of stress–strain curves obtained by samples geometries according to EN 10002-1 and micro-flat tensile samples. As reference material, high purity copper rolled to 70% in thickness reduction and cold rolled and annealed copper (1 h at 350 °C) was used.

and after etching investigated by optical microscopy (OM). A more detailed view on micro-mechanisms of the failure and fracture morphologies is supplied by scanning electron microscopy (SEM) of fractured surfaces.

3. Experimental results

3.1. Applicability of micro-flat tensile tests to determine mechanical properties of pure copper

The results presented in Fig. 2 and Table 2 demonstrate that miniaturized test samples show slightly higher yield strengths for the highly deformed and the annealed state and very similar ultimate strengths for both conditions. In that comparison, the miniaturized test samples also show a higher elongation to failure than the samples tested according to EN 10002-1. Those differences might be attributed to a slightly more non-uniform deformation of the small geometries, but within the given range justify to use such 'micro-flat' tensile samples to determine mechanical properties of cold-sprayed and thermally sprayed coatings.

Table 2
Mechanical data obtained for cold rolled and for additionally annealed bulk copper in tensile tests according to EN 10002-1 and by micro-flat tensile specimen geometries

Sample type	Yield strength (MPa)	Ultimate strength (MPa)	Elongation to failure (%)
EN 10002-1, Cu, cold rolled	378.0±2.0	390.0±0.6	2.63±0.06
Miniaturized sample Cu, cold rolled	360.3±1.5	384.7±0.2	3.00±0.28
EN 10002-1, Cu, cold rolled and annealed	62.7±0.6	231.3±0.6	43.67±0.58
Miniaturized sample Cu, cold rolled and annealed	73.0±1.0	229.6±0.5	49.67±1.53

3.2. Mechanical properties of cold-sprayed copper coatings

The data from tensile tests of the various coatings and heat-treated states concerning the maximum strength, yield strength and elongation to failure were determined as mean value from minimum three measurements and parts of that are summarized in Table 3. In most of these measurements, the data in the linear elastic region scattered over an extremely large range, making it impossible to extract reliable data for the determination of the Young's modulus. As far as a transition to plastic flow was observed, respective yield strengths ($R_{p0.2}$: according to EN 10002) are reported. As demonstrated by the data in Table 3 for the as-sprayed conditions, no significant differences within the attainable range of errors were obtained for samples cut from sites close the surface (top), the middle of the coating (middle) or sites close to the substrate (bottom). The data for the various annealing states show an even more uniform appearance for different layer sites, which, therefore, are not explicitly presented in the current work. Data for the different annealing stages of the various coatings are shown for the 'middle' layers, as indicated in Fig. 2. It is also worth noting that none of the investigated samples showed pronounced necking.

Examples of typical stress–strain curves as obtained from the tensile tests for as coated and for later annealed copper coatings, sprayed with nitrogen as process gas, are shown in Fig. 3. The curves demonstrate the significant influence of the heat treatment on mechanical properties. As shown in Table 3, a mean value of about 45 MPa was obtained for the ultimate strength in the as-sprayed state, in line of the spray tracks. For those samples, which had been cut perpendicular to the spray tracks, an ultimate strength of 80 MPa was measured. However, since the amount of the latter type of specimens was rather limited, no further information on anisotropy effects on annealing was investigated. The elongation to failure did not exceed 0.1% for any of the samples sprayed with nitrogen as process gas. Annealing the specimens for 1 h at 200 °C prior to the tests caused an increase in ultimate strength to about 85 MPa in line to the spray tracks, which already improved the initial strength by more than 50%. Nevertheless, the elongation to failure was still very low. By the subsequent annealing for 1 h at 400 °C, maximum strength and the elongation to failure were improved to 170 MPa and 0.5%, respectively. The yield strength of that annealing state was determined to about 150 MPa. By annealing at 600 °C, mechanical properties of nitrogen-sprayed copper coatings can be further improved and reach an ultimate strength of about 210 MPa and 8% elongation to failure. The yield strength of about 165 MPa is quite similar to that after annealing at 400 °C.

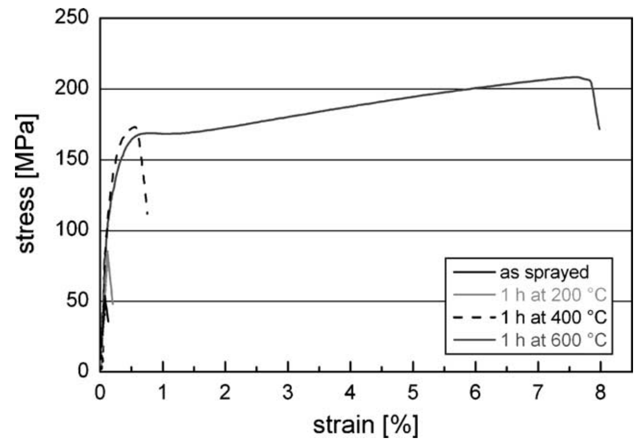

Fig. 3. Stress–strain curves of cold-sprayed coatings produced with nitrogen as process gas after different heat treatments.

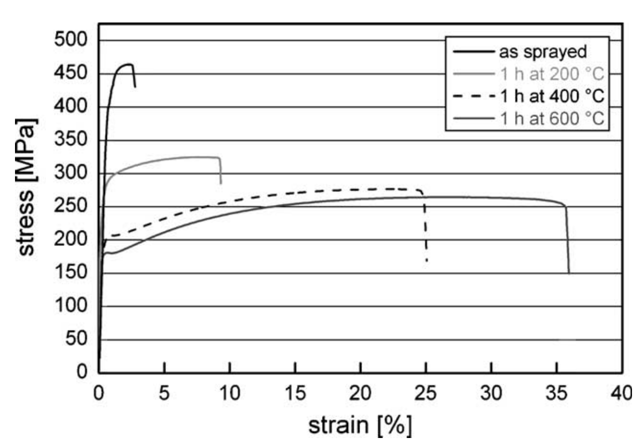

Fig. 4. Stress–strain curves of cold-sprayed coatings produced with helium as process gas after different heat treatments.

Table 3
Mechanical data of cold, HVOF and arc-sprayed (a.s.) coatings as obtained after different heat treatments

Sample type	Position in sample	Annealing condition	Yield strength (MPa)	Ultimate strength (MPa)	Elongation to failure (%)
CS, N_2, in line	Top	a.s.	–	26±21	<0.1
	Middle	a.s.	–	46±12	<0.1
	Bottom	a.s.	–	33±6	<0.1
	Middle	200 °C	–	86±1	0.12±0.00
	Middle	400 °C	150	171±4	0.51±0.12
	Middle	600 °C	165	210±6	8.03±2.16
CS, N_2, perpendicular	Top	a.s.	–	87±1	<0.1
	Middle	a.s.	–	80±8	<0.1
	Bottom	a.s.	–	77±20	<0.1
CS, He, in line	Top	a.s.	–	472±2	2.31±0.15
	Middle	a.s.	403	453±16	1.92±0.63
	Bottom	a.s.	–	454±3	2.47±0.29
	Middle	200 °C	255	304±29	4.27±5.19
	Middle	400 °C	193	278±2	20.99±1.42
	Middle	600 °C	172	262±4	23.85±3.82
HVOF, in line	Top	a.s.	–	140±10	0.20±0.04
	Middle	a.s.	–	146±5	0.23±0.03
	Bottom	a.s.	–	151±10	0.25±0.05
	Middle	200 °C	–	132±18	0.21±0.06
	Middle	400 °C	–	144±6	0.25±0.04
	Middle	600 °C	125	129±5	0.43±0.12
AS, in line	Top	a.s.	–	96±7	0.28±0.02
	Middle	a.s.	–	93±10	0.26±0.02
	Bottom	a.s.	–	102±6	0.36±0.02
	Middle	200 °C	–	104±4	0.30±0.02
	Middle	400 °C	–	95±5	0.30±0.02
	Middle	600 °C	65	68±4	0.31±0.09

For each condition, minimum of three measurements were performed.

Respective stress–strain plots of typical as-sprayed and of annealed copper coatings, sprayed with helium as process gas are given in Fig. 4. As summarized in Table 3, the coatings, sprayed with helium as process gas already show a quite high ultimate tensile strength of about 450 MPa in the as-sprayed state. Moreover, the elongation to failure reached 2%. The mean yield strength is determined to about 400 MPa. As expected for highly deformed material, the yield strength, the ultimate strength decrease and the elongation to failure increase with rising annealing temperatures. Respectively, annealing at a moderate temperature of 200 °C already results in a twice as high elongation to failure (4%), as compared to the as-sprayed condition. After annealing at 400 °C, the yield strength and the ultimate strength are decreased to 190 MPa and 280 MPa, respectively. The elongation to failure exceeds 20%. After the heat treatment at 600 °C, a yield strength of 170 MPa and an ultimate strength of 260 MPa were obtained. At that annealing temperature, the elongation to failure reaches about 24%.

3.3. Mechanical properties of thermally sprayed copper coatings

HVOF-sprayed coatings show an ultimate tensile strength of 145 MPa and an elongation to failure of about 0.2% in the as-sprayed state (Table 3). As compared to the initial condition, the ultimate tensile strength and the elongation to failure have not significantly changed after annealing at 200 °C and at 400 °C. Just after annealing at 600 °C, a notable decrease in strength to about 130 MPa and a slight increase of elongation to failure to about 0.4% were observed. The yield strength for that annealing condition can be determined to 125 MPa.

In the as-sprayed state, arc-sprayed coatings show an ultimate strength of about 95 MPa and an elongation to failure of 0.3%. Neither strength nor elongation to failure can be improved by annealing at 200 °C or 400 °C. After the heat treatment at 600 °C, the ultimate strength is reduced to 70 MPa, whereas the elongation to failure still does not exceed 0.3%. For that annealing condition, the yield strength can be estimated to 65 MPa.

3.4. Fracture morphologies of micro-flat bulk copper samples

In order to gain detailed information on the micro-mechanisms of the deformation behaviors of the coatings and the type of failure in small geometries, the fracture surfaces of various micro-flat tensile samples were analyzed by OM in cross-section and by SEM in top view. Since work hardening or surface treatments by spark erosion might influence the attainable pattern, typical features of cold rolled and soft annealed samples are given as examples. Both the investigated bulk samples according to EN 10002-1 and the 'micro-flat' samples show pronounced necking and shear fracture at an angle of about 45° to the applied tensile stress. For micro-flat sample geometries, Fig. 5 displays fracture microstructures and morphologies of bulk copper (Cu 99.99%), cold rolled to 70% in thickness reduction and of cold rolled and heat-treated copper sheets (1 h at 350 °C). For the hard, cold rolled state, necking is, as expected, less pronounced (Fig. 5a) than for the soft, annealed state (Fig. 5b). Fracture surfaces of both micro-flat tensile test samples show the typical dimple pattern of ductile fracture. The pattern sizes of typically 10 μm correlate to the few oxides present in the samples. As typical for cold worked material, the dimples are flatter for the cold rolled copper sample. As a summary, the fracture morphologies observed in micro-flat

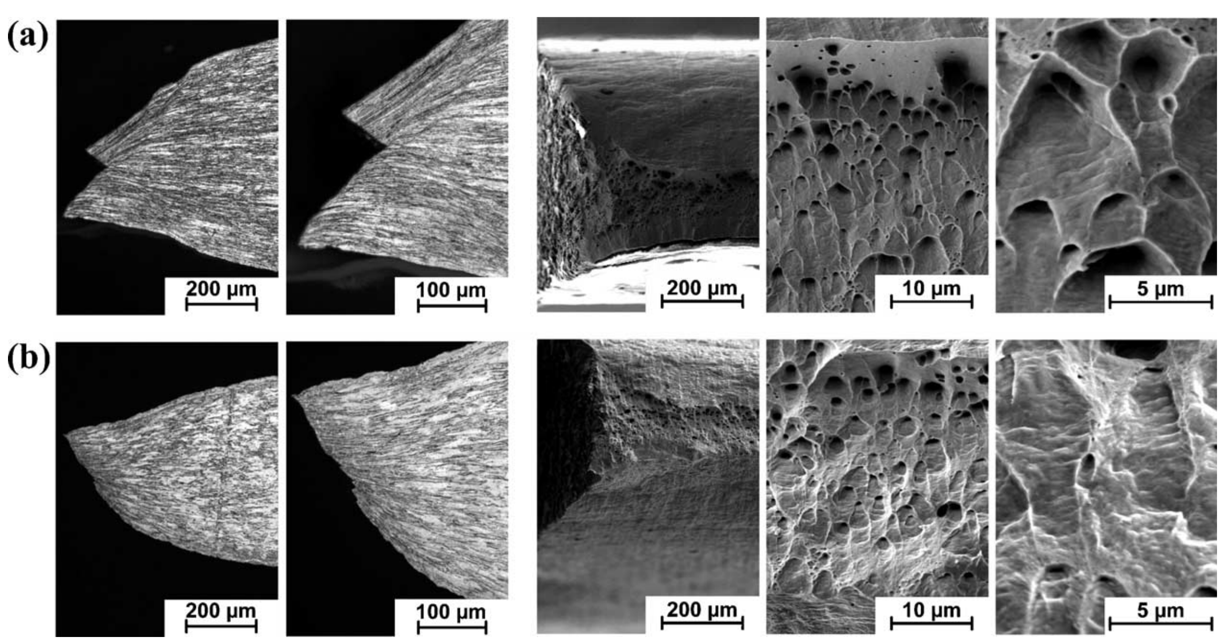

Fig. 5. Fracture microstructures and surfaces of bulk copper (Cu 99.99%), (a) cold rolled to 70% in thickness reduction and (b) of cold rolled and heat treated copper sheets (1 h at 350 °C). The micrographs on the left side show etched cross-sections of broken micro-flat tensile test samples. On the right side, details of fracture surfaces as obtained by SEM analysis (SE-mode) are displayed.

specimens reveal no differences to bulk samples according to EN 10002-1 and thus underline that micro-flat geometries can be used to determine the mechanical properties of copper coatings.

3.5. Fracture morphologies of cold-sprayed copper coatings

Fig. 6 summarizes the microstructures and fracture surface morphologies of the cold-sprayed coatings, processed with nitrogen as propellant gas, for the as-prepared state (Fig. 6a) and for annealing temperatures of 400 (Fig. 6b) and 600 °C (Fig. 6c). Fracture morphologies of samples, which are annealed at 200 °C, are very similar to the as-sprayed condition and are thus not shown in separate micrographs. For the as-sprayed state, the OM micrographs of the rupture surface reveal cleavage fracture, perpendicular to the applied stress (Fig. 6a). Failure is mainly initiated at interfaces between the flattened spray particles. The cross-sectional, optical micrographs also reveal cracks inside the sample or close to the surface, which probably formed during the deformation. More details are exposed by the SEM micrographs of fracture surfaces. Around the areas of crack initiation at particle–particle interfaces, regions are visible which have an appearance similar to trans-granular cleavage fracture of strain-hardened metals. These regions cover about 10% to 20% of the fracture surface. OM micrographs of coatings, which were annealed at 400 °C before testing, show that fracture to a certain extent occurs angular to the applied stress (Fig. 6b). Individual spray particles appear to be strained before failure and some of them show trans-granular failure. As compared to the as-sprayed state, less cracks are present inside the coating. SEM micrographs still reveal features of former spray particles (Fig. 6b). The closer view demonstrates that failure at inter-particle boundaries is governed by dimple pattern. In addition, trans-granular dimple rupture can be observed. Nothing of both was monitored for the as-sprayed state or for coatings annealed at 200 °C. Typical dimple sizes range from 0.2 μm to about 0.6 μm. Samples that were annealed at 600 °C before the tensile test show fracture topographies, for which failure at former particle–particle interfaces is less prominent (Fig. 6c). According to the cross-sectional micrographs, former spray particles are strained under the applied load and most of them rupture trans-granular. Overall, crack propagation occurs angular to the strained direction. SEM analyses reveal that most of the fracture surface is covered by trans-granular dimple pattern. Trans- and inter-granular dimple sizes typically range from 1 to 5 μm. Small angular

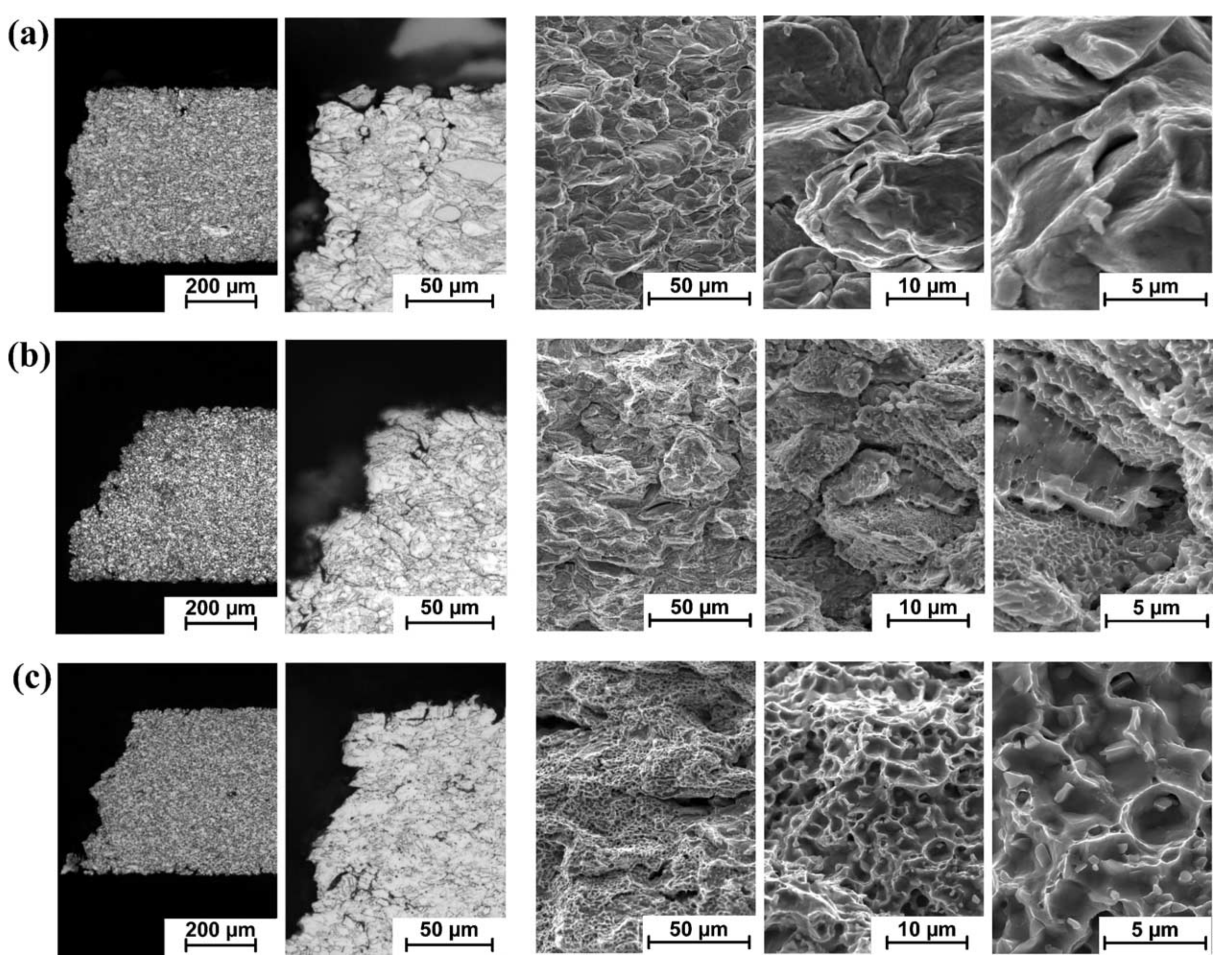

Fig. 6. Fracture microstructures and morphologies of CS coatings, sprayed with N_2 as process gas: (a) as-sprayed, (b) annealed for 1 h at 400 °C, (c) annealed for 1 h at 600 °C. The micrographs on the left side show etched cross-sections of broken micro-flat tensile test samples. On the right side, details of fracture surfaces as obtained by SEM analysis (SE-mode) are displayed.

precipitations at the bottom of dimple sites can often be identified as origin of fracture. EDS analysis reveals that such failure is associated with the appearance of copper oxides, initiating crack propagation. Overall, the amount of ductile failure comprises almost 100% of the surface.

Fracture morphologies of cold-sprayed coatings, processed with helium, are shown in Fig. 7. In the as-sprayed state (Fig. 7a), fracture occurs angular to the applied stress and most of the spray particles appear to be strained before failure, as indicated by the OM micrographs. Apart from those at the failure surface, no cracks are detected inside the sample. The SEM micrographs reveal a more uniform surface topography than for the coating sprayed with nitrogen as process gas. Details of the fracture morphology reveal additional differences with respect to the nitrogen-sprayed coating. Features of plastic deformation dominate the topography. Typical sizes of 5 to 10 μm are more than two times smaller as the initial particle diameters, and can be mainly attributed to trans-particle failure. The type of pattern appears similar to rupture features of heavily strain hardened bulk material. Respective ductile failure appears to cover about 80% of the fracture surface. Brittle fracture at particle–particle interfaces appears to cover less than about 10% to 20% of the rupture surface. Although respective micrographs are not shown here, it is worth noting that the fracture surface of coatings annealed at 200 °C shows a quite similar appearance to that of the as-sprayed state, despite the higher elongation to failure obtained in the tensile test. The coatings, which were sprayed with helium and heat-treated at 400 °C, show fracture surfaces with quite uniform morphologies, making it difficult to distinguish individual spray splats (Fig. 7b). The OM micrographs of the cross-section reveal highly elongated features in the fracture surface. Underneath the fracture surface, various other sites of crack initiation are observed. The SEM micrographs demonstrate that the amount of ductile failure covers nearly the complete surface with quite a wide variety of different dimple features. The smallest of them have sizes of typically 1 μm. Thus, as compared to the same annealing condition of the coatings sprayed with nitrogen as process gas, the fracture morphology is not only smoother, it also shows larger dimple pattern. For the annealing state of 600 °C (Fig. 7c), OM micrographs of the cross-section reveal fibrous features in strain direction. For the coating itself, no sign of former particle–particle interfaces can be exposed by etching. SEM micrographs show that surface topographies are more uniform; as compared to the heat treatment at 400 °C.

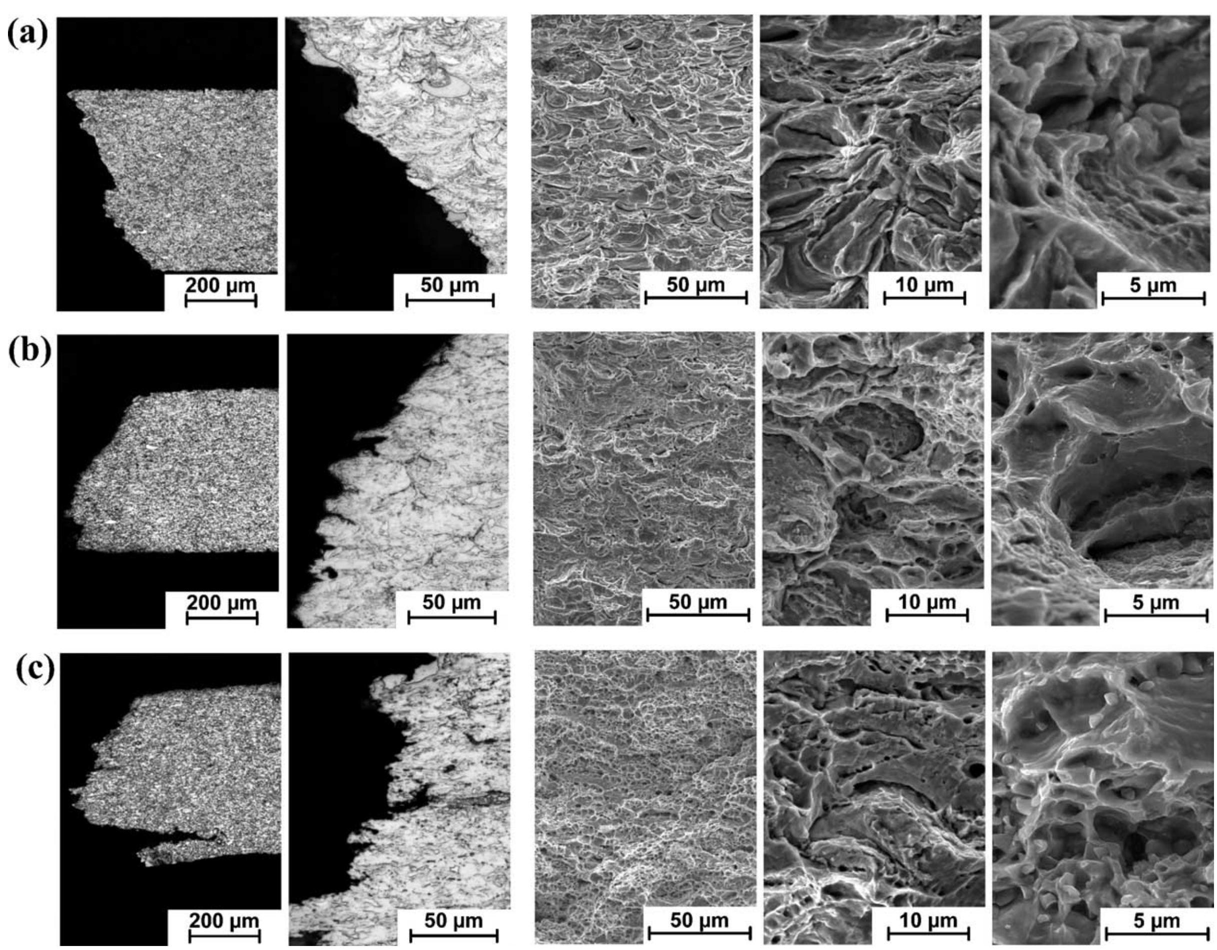

Fig. 7. Fracture microstructures and morphologies of CS coatings, sprayed with He as process gas: (a) as-sprayed, (b) annealed for 1 h at 400 °C and (c) annealed for 1 h at 600 °C. The micrographs on the left side show etched cross-sections of broken micro-flat tensile test samples. On the right side, details of fracture surfaces as obtained by SEM analysis (SE-mode) are displayed.

Dimple sizes are larger and range from about 1 to 5 μm. Thus, dimple pattern cover a larger size range than that of fracture surfaces of identically treated coatings, sprayed with nitrogen as process gas.

3.6. Fracture morphologies of thermal spray coatings

OM and SEM micrographs of fracture surfaces of HVOF-sprayed coatings are summarized in Fig. 8 for different annealing conditions. In the as-sprayed state (Fig. 8a), according to the OM micrographs of the cross-section, fracture occurred in an angle, not perpendicular the stress direction. Details reveal quite non-uniform features with failure at former spray splat interfaces and highly fragmented sites of crack propagation. Particularly, the latter seem to be subject of ductile deformation. Underneath the fracture surface, crack branches spread into a depth of about 100 μm into the specimen and sites of crack propagation appear to be related to oxidic features between spray splats. As shown by SEM, the fracture surface of the as-sprayed HVOF coating is quite rough and reveals features of brittle rupture on spray splat surfaces and ductile trans-granular failure (Fig. 8a). According to OM and SEM analyses, areas of brittle inter-particle failure cover about 30–40% of the fracture surface. Moreover, etched cross-sections and surface morphologies demonstrate that in HVOF spaying a significant amount of spray particles is impacting in the solid state. Areas of trans-granular rupture show ductile dimple and brittle cleavage fracture which spread over scales of typically 5 to 10 μm. Respective regions seem to originate from splats that impacted in the liquid state and rapidly solidified on the substrate. In these areas, dimple sizes range from about 0.1 to 0.5 μm. Fracture surfaces of HVOF-sprayed coatings, annealed at 200 °C, are very similar to those of the as-sprayed state and are therefore not presented. Moreover, HVOF-sprayed samples, annealed at a temperature of 400 °C before tensile testing (Fig. 8b), show fracture morphologies, which are quite similar to those of the as-sprayed condition. The OM micrographs reveal as well ductile, fragmented shear failure angular to the applied stress, as brittle rupture, perpendicular to the strain direction, at interfaces of spray particles that impacted in the solid state. Crack branches around the more fragmented regions spread into a depth of about 50 μm below the fracture surface, and other cracks started to form in a larger distance. The etched cross-section also reveals that oxide layers around former spray splats are still retained at a annealing temperature of 400 °C. The SEM micrographs of the fracture surface mainly confirm above

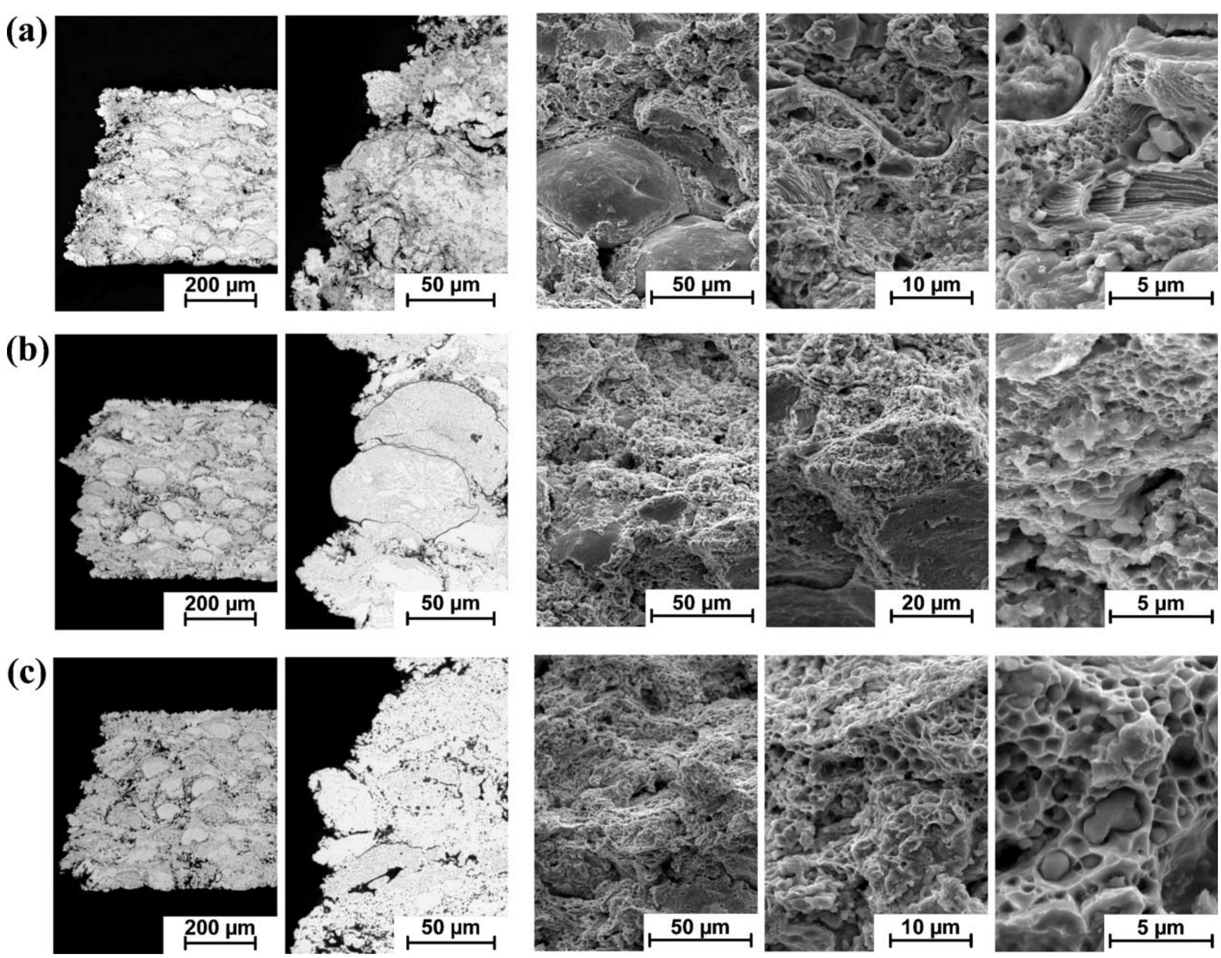

Fig. 8. Fracture microstructures and morphologies of HVOF-sprayed coatings: (a) as-sprayed, (b) annealed for 1 h at 400 °C and (c) annealed for 1 h at 600 °C. The micrographs on the left side show etched cross-sections of broken micro-flat tensile test samples. On the right side, details of fracture surfaces as obtained by SEM analysis (SE-mode) are displayed.

results. In addition, the detailed view under higher magnification demonstrates that dimple sizes of typically 0.3 to 1 μm in more ductile regions are slightly larger than those of the as-sprayed state or after annealing at 200 °C. The fracture surface of the coating, annealed at 600 °C before testing (Fig. 8c), is as well quite rough and to a small extent retains features of the original splats. According to OM micrographs of the etched cross-section, the surface is rather fragmented and is showing failure along sites of oxide distribution. Below the fracture surface, other sites of crack initiation are visible mainly in areas of higher oxide concentration. SEM analyses of the fracture morphology demonstrate that ductile dimpling is more prominent than for the heat treatment at 400 °C. Only a negligible amount of the fracture surface shows brittle inter-particle rupture. Nevertheless, the fracture surface still retains pattern on length scales of sizes similar to those of the powder feedstock. Thus, most of the pattern can interpreted similar to ductile inter-particle fracture, due to the presence of spheroidized oxides as crack initiation centers. Dimple sizes of typically 1 to 3 μm are much smaller than for cold-sprayed coatings after similar heat treatments, just reflecting the higher amount of oxides and their stronger localization. That difference might be attributed to dissolved oxide shells on former HVOF spray particles or splats and might explain the low elongation to failure.

Fig. 9 displays typical features of fracture surfaces of as prepared and annealed arc-sprayed coatings. The OM micrographs of etched cross-sections for the as-sprayed condition illustrate different oxygen contents in spray splats, retained oxide layers that appear to act as centers of crack initiation and failure, and in-between strained ductile regions (Fig. 9a). Areas which are more ductile are strained during deformation and show fragmented failure surfaces. This plastic deformation of metallic regions seems to carry most of the overall load, whereas cracks easily spread through oxide layers. That also might explain the non-perpendicular angle of the failure surface with respect to the applied stress. The micrographs also reveal secondary crack nucleation sites far below the actual fracture surface, in correlation with the appearance of oxides and some pores. As analyzed by SEM (Fig. 9a), the fracture surface of the arc-sprayed coating is quite rough and shows a lamellar morphology of metallic components and oxide layers, which is specific for this spray process. EDS analyses confirm that brittle fracture at comparatively smooth lamellas can be attributed to oxides. In the as-sprayed state, these lamellas cover about half of the fracture surface. Areas in-between

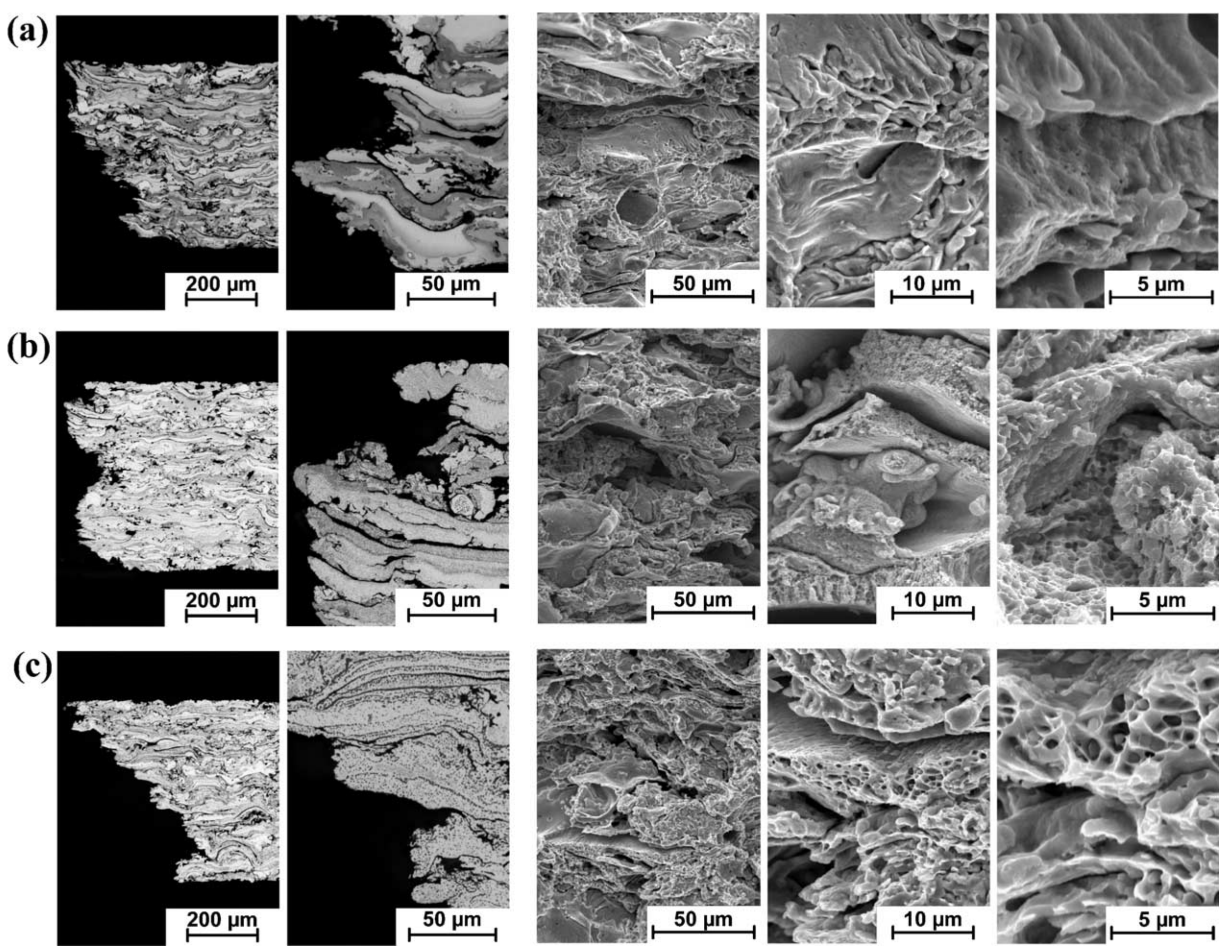

Fig. 9. Fracture microstructures and morphologies of arc-sprayed coatings: (a) as-sprayed, (b) annealed for 1 h at 400 °C, (c) annealed for 1 h at 600 °C. The micrographs on the left side show etched cross-sections of broken micro-flat tensile test samples. On the right side, details of fracture surfaces as obtained by SEM analysis (SE-mode) are displayed.

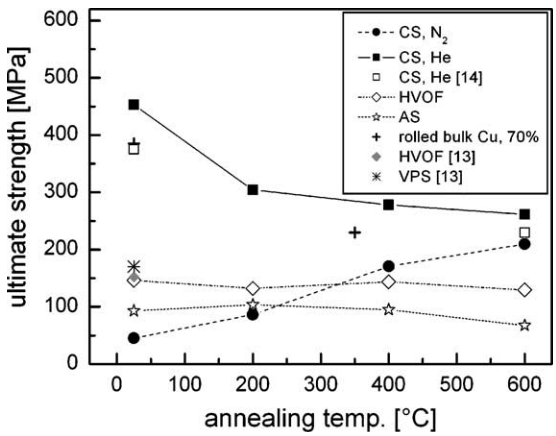

Fig. 10. Ultimate strength of cold-sprayed and thermally sprayed copper coatings for the as-sprayed state and various annealing temperatures. For comparison, data for cold rolled copper are also included in the graph.

lamellas show some ductile deformation resulting in quite irregular shapes and features of inter granular cleavage and to a minor extent dimple fracture. As observed, dimple patterns appear on very small length scales and have sizes of typically less than 0.1 μm. Samples that were heat-treated at 200 °C display identical features as the as-sprayed state and are therefore not explicitly shown for comparison. Fracture surfaces of AS coatings (Fig. 9b), which were annealed at 400 °C, despite the similar performance in tensile testing in comparison to as-sprayed coatings, show quite different microstructures and morphologies. Contours of oxygen distributions, as observed by OM, are sharper due to finely dispersed oxides, and surfaces appear to be less fragmented as for the as-sprayed state. Failure initiation is most prominent at oxide layers and the formation of additional cracks near to the fracture surface is rather limited. The SEM micrographs of the fracture surface of the coating, annealed at 400 °C, reveals that the areas between the lamellas to a higher extent show ductile dimple fracture (Fig. 9b) than those of the as-sprayed state. Dimple pattern are quite regular with sizes from 0.3 to 0.6 μm. Nevertheless, inter-splat cleavage can still be observed. Overall, the amount of ductile fracture covers about a third to a half of the rupture surface. Fracture microstructures and morphologies of the AS coating, heat-treated at 600 °C are shown in Fig. 9c. The OM micrographs reveal fracture in an angle of 45° to the direction of applied stress, indicating plastic deformation before failure. In comparison to the heat treatment at 400 °C, lamellar oxide layers are thinner and fine dispersed precipitations are larger. The latter are mainly aligned along former splat boundaries or oxide layers. As compared to the as-sprayed state or heat treatments at lower temperatures, the formation of cracks behind the failure front is less prominent. The more detailed SEM analyses reveal quite similar fracture surfaces as for the annealing stage at 400 °C (Fig. 9c). The major difference to the heat treatment at 400 °C is given by the larger dimple sizes of about 1 to 2 μm. By the high annealing temperature, the number of sites for brittle failure can be reduced, but as shown in the comparison to cold spraying or HVOF spraying, the amount of available crack initiation centers in ductile failure can also significantly influence crack formation and propagation.

4. Discussion

4.1. Coating performance

Fig. 10 summarizes the tensile strengths (Tables 2 and 3) for the different coating and annealing conditions. The decrease of ultimate strength with increasing annealing temperature of CS copper coatings, sprayed with helium as process gas is similar to that of bulk material cold rolled to 70% in thickness reduction (%). The slight differences can be attributed to the higher degree of work hardening, attained by cold spraying with helium. Taking hardness as a measure for strain hardening by cold working, the amount of deformation in cold spraying correlates to 90% reduction in thickness by cold rolling [7]. The observed strength of the as-sprayed state also agrees well to that of copper wires, cold drawn to 85% in size reduction, which show an ultimate strength of 455 MPa [18]. The slightly lower strength reported in literature for copper coatings processed with helium [14] might be attributed to different parameter settings in cold spraying. In contrast to deformed bulk copper or coatings, processed with helium, the strength of coatings, cold-sprayed with nitrogen, increases with annealing temperature, whereas strengths of thermally sprayed coatings are only negligibly affected by following heat treatments. In the as-sprayed state, the ultimate strength of HVOF-sprayed copper coatings agrees well to values reported in literature [13]. It is also worth noting that vacuum plasma-sprayed coatings show a slightly higher ultimate strength than HVOF-sprayed coatings [13]. Since none of the tensile test samples prepared from coatings showed necking, failure is attributed to intrinsic defects, which act as initial cracks of over critical size, being responsible for the brittle behavior of most of the as-sprayed coating.

Fig. 11 compares the elongation to failure for the different coatings and rolled bulk material attained after different heat treatments. In the as-sprayed state, the coating, processed with helium as propellant gas, reaches an elongation to failure,

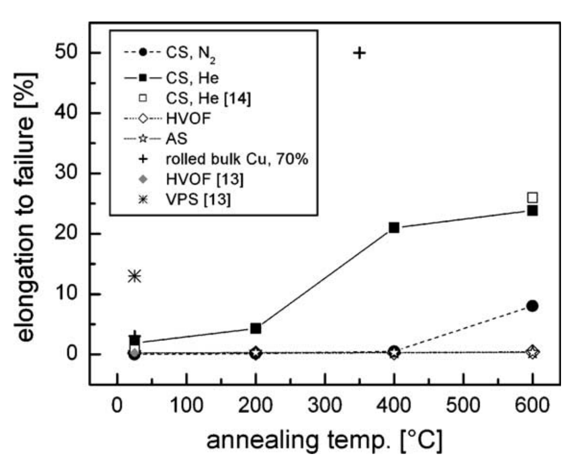

Fig. 11. Elongation to failure of cold-sprayed and thermally sprayed copper coatings for the as-sprayed state and various annealing temperatures. For comparison, data for cold rolled copper are as well included in the graph.

which is quite similar to that of cold rolled bulk material. With subsequent annealing, the attainable strain can be enhanced to about maximum 25%, which is about half of the elongation observed for soft annealed bulk copper. This indicates that, after annealing, microstructural defects are still present, which can limit further deformation. For the cold-sprayed coating, processed with nitrogen, a substantial increase of elongation to failure requires annealing temperatures of 400 °C or more. In contrast, the attainable maximum strain of HVOF coatings and arc-sprayed coatings cannot be affected by the various heat treatments. For any type of coating and annealing condition, the attainable elongation is thus limited by the maximum size of present non-well-bonded areas, which allow crack propagation. As reported in literature, VPS coatings in the as-sprayed state show a substantially higher elongation to failure than cold-sprayed, HVOF-sprayed or arc-sprayed coatings [13].

4.2. Influences of coating microstructures

The described differences in properties can be explained by coating microstructures obtained in cold spraying and thermal spraying [7]. By the impact of solid particles in cold spraying, micro-structural features are determined by highly deformed, flattened spray splats. Bonding of spray particles is attributed to shear instabilities by thermal softening, which spread from the outer rim of the impact crater towards the point of initial contact [5]. Occurring material jets clean respective interfaces from oxides and guarantee intimate metallic bonding. After tensile rupture, these well-bonded areas show ductile fracture morphologies, similar to bulk material. Nevertheless, the occurring shear instabilities in cold spraying will leave an area around the point of initial contact of impacted particles, which is only subject to cold forging under compression [5,7]. Due to substantially higher impact velocities, the amount of well-bonded particle–particle interfaces can be increased from about 20% to about 80% by spraying with helium instead of nitrogen as process gas [7]. Moreover, in coatings processed with helium, highly deformed areas spread deeper into particle cores than in coatings sprayed with nitrogen.

During annealing, the microstructural development of cold-sprayed coatings should be determined by recovery and diffusion-driven processes like recrystallization and spheroidization of planar inter-particle defects. The particle temperature by cold spraying with helium is lower than by spraying with nitrogen. A higher impact temperature might allow more deformation due to easier softening, but also can contribute to recovery already during the coating process and, thus, to reduced dislocation densities. For the helium-sprayed coating with already bulk-like properties in the as-sprayed state, hardness decreases with increasing annealing temperature, as reported in Stoltenhoff et al. [7], due to the declining number of dislocations, and results in the reduction of the ultimate strength. Cold-sprayed copper coatings, processed with nitrogen as process gas, to a higher extent, show particle–particle interfaces, which are just cold forged. Under tensile stress, respective areas can act as crack centers with over critical size. Thus, rupture in the as-sprayed state mainly occurs at particle–particle interfaces. As for coatings sprayed with helium, annealing of the coatings processed with nitrogen results in recovery and recrystallization and decreased hardness [7]. In addition, the diffusion during the heat treatments reduces the amount and sizes of interfaces not being metallurgically bonded. Thus, potential nucleation sites for crack formation are decreased. As a consequence, the ultimate strength is increased with increasing annealing temperatures. On corresponding fracture surfaces, dimple patterns, being characteristic for ductile failure, are getting more prominent. After a heat treatment at 400 °C or more, strengths are reached, which are similar to those of soft annealed bulk copper (Fig. 10) and ductile failure occurs on most of the rupture surface. Nevertheless, after annealing the coating sprayed with nitrogen as process gas at 400 °C, the elongation to failure is still quite low, due to non-bonded areas, still present after annealing (Fig. 11). Diffusion length scales are probably too short to close all more open, not on atomic-scale bonded, areas. After annealing at 600 °C, potential sites for crack initiation are drastically reduced, allowing substantial plastic deformation of the tensile test samples. Fracture morphologies reveal ductile failure with dimple sizes, which are larger than those obtained after annealing at 400 °C and indicate an increase in the free path for crack evolution. Larger dimple sizes can be attributed to the growth of oxides and thus larger distances between them. Since diffusion reduces the number of all sorts of internal defects in cold-sprayed coatings, annealing improves also their electrical conductivity. After a heat treatment at 600 °C, the electrical conductivity measured at room temperature of the coating sprayed with nitrogen reaches 90% of that attained for soft annealed bulk material [7,19].

Brittle rupture can also occur at interfaces between metallic splats and oxides or within oxides, as shown for the example of arc-sprayed and HVOF-sprayed coatings. As illustrated by the fracture surfaces, metallic items mainly show trans-granular rupture. Crack ignition and propagation is most prominently located at interfaces between metallic and oxidic features of the lamellar appearing spray splats. Thus, the distribution of these oxides should play a major role with respect to the mechanical properties of these coatings. Under the applied tensile loads in the plane of coatings, the mechanical properties should be determined by the shear strength of internal, lamellar interfaces. In thermal spray processes, the spray material is completely molten as in arc spraying or at least partially molten as in HVOF spraying. Oxidation can occur during the flight through the nozzle and the free gas jet and also can take place during solidification on the substrate [20]. Respective contributions to coating microstructures are dependent on the chemistry of the spray material, the achieved temperatures and exposure times. In the as-sprayed state, arc-sprayed copper coatings show microstructural features with oxide layers and areas that are highly supersaturated with oxygen [7]. HVOF-sprayed coatings show quite different contours of contrast [7], indicating a steeper gradient in the oxygen concentration, which can be mainly attributed to the lower temperature of semi-solid impacting particles. For the as-sprayed state, these differences result in a tensile strength of the HVOF-sprayed coatings, which is substantially higher than that of arc-sprayed coatings or than that of nitrogen processed cold-sprayed coatings (Fig. 10). These differences can be attributed to a higher amount of metallic bonds within the HVOF coatings. As compared to HVOF-sprayed or arc-sprayed copper, the higher ultimate strength and elongation to failure of VPS coatings can be attributed to the low lower amount of embedded oxides and the high substrate temperatures and thus annealing during the coating process [13].

Since defects introduced by mechanical deformation are less prominent for thermal spray coatings, annealing should mainly result in the precipitation and the rearrangement of oxides by atomic diffusion. As pointed out in previous work, diffusion in thermal spray coatings should be less effected by non-equilibrium vacancies, interstitials, dislocations or more open internal interfaces than for cold-sprayed coatings [7]. During annealing of thermal spray coatings, the short length scales of atomic bulk diffusion result in small, spheroidized oxides, which are mainly aligned at interfaces of former spray droplets or in line at certain levels of oxygen concentration inside spray splats. Whereas the electrical conductivity can be significantly improved by the annealing of thermal spray coatings [7], the ultimate tensile strengths are only slightly affected by heat treatments at temperatures of up to 600 °C. That difference can be attributed to the distribution and typical length scales of defects and their rearrangement during annealing. The electrical conductivity is substantially influenced by scattering sites for electrons on atomic scales, given by the oxygen content in solid solution, sub-micron phase boundaries or ultra high dislocations densities. Short-range diffusion is sufficient to precipitate oxides, to reduce the supersaturation with oxygen and to decrease the number of point defects and dislocations. An increase in tensile strength, however, requires a decreased amount of potential, larger crack nucleation sites. The spheroidization of oxides on the one hand enlarges the overall amount of metallic bonds between spray splats, but on the other hand might also increase the number of available sites for crack nucleation. Length scales for diffusion to coagulate formerly flattened oxides should be one of the main factors determining attainable thermal spray coating properties.

The distance of crack initiation centers like oxides determines dimple sizes in ductile areas. The more ductile failure of annealed thermal spray coatings in closer view demonstrates the detrimental influence of aligned, fine dispersed oxides, which are present at former spray splat interfaces. The distance between them is obviously too small to allow substantial ductile deformation of the surrounding metallic matrix. The present results show that the ultimate strength of HVOF- and arc-sprayed coatings cannot be improved by annealing at economically justifiable temperatures of up to 600 °C.

4.3. Differences to bulk material

Additional information on the deformation behaviour can be gained by correlating yield strength and hardness, as shown in Fig. 12. Taking data from literature for differently deformed bulk copper [21] and pre-deformed and later annealed material from the current study, the yield strength gives a linear function of hardness. For the comparison with cold-sprayed and thermally sprayed coatings, hardness data from a previous publication were used [7]. Cold-sprayed coatings show a quite good agreement to the bulk material in comparatively soft states, i.e. after annealing at 400 or 600 °C. As demonstrated by the coatings sprayed with helium as process gas, with increasing hardness, the measured yield strength increasingly deviates from the ideal correlation. The lower yield strength of cold-sprayed coatings, at same hardness as compared to the bulk material, can be attributed to the highly non-uniform microstructures and deformation pattern obtained in the as-sprayed state. Whereas hardness measurements average over all features in a couple of spray particles, the yield strength will be determined by the softest, i.e. means minimum work hardened local areas. With increasing annealing temperatures and respectively lower hardness, local microstructural differences decline and the cold-sprayed coatings behave very similar to the bulk material. Interpreting the comparison as a measure for non-uniform microstructures, the coating sprayed with helium as process gas at a hardness of 100 HV 0.3, which corresponds to an annealing temperature of 200 °C, should already show a very homogeneous microstructure. As far as measurable, the yield strengths of annealed cold-sprayed coatings processed with nitrogen, seem to show a slightly larger deviation and therefore less uniform microstructures. Within the current set of annealing temperatures of up to 600 °C, neither yield strength nor hardness could be reduced to similar values as obtained for deformed and soft annealed bulk copper. These differences can be explained by the occurrence of persistent dislocation loops, which were formed by the condensation of point defects obtained in high strain rate deformation [8]. At a hardness of about 75 HV 0.3, the HVOF-sprayed coating, soft annealed at 600 °C, is showing significantly lower yield strength than bulk copper or cold spray coatings. That can be attributed to additional non-uniform microstructural features, apart from dislocation loops, probably oxides, which reduce coating performance. The reduced yield strength, for example,

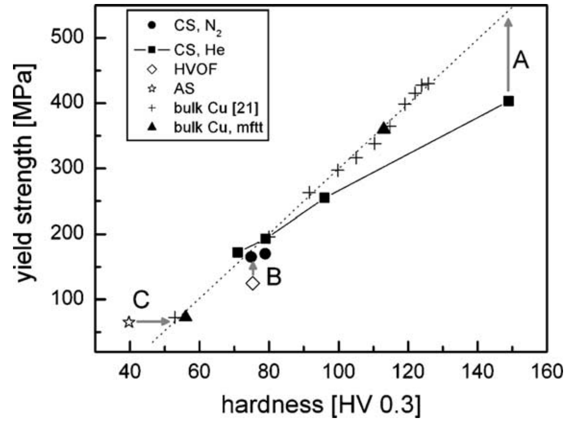

Fig. 12. Correlations between yield strength and hardness for cold rolled bulk copper and copper coatings. Deviations from bulk properties are indicated by arrows for cold-sprayed coatings, processed with helium (A), HVOF-sprayed coatings (B) and arc-sprayed coatings (C). Results from microflat tensile tests of bulk material are referred by the abbreviation 'mftt'.

could be explained by a smaller amount of microstructural features, which show ductile deformation, as compared to the overall cross-section. For soft annealed arc-sprayed coatings, the correlation deviates in opposite direction showing a higher strength under tensile loads as compared to compressive loads in hardness testing. The comparably low hardness might be explained by porosity. Moreover, it has to be considered that the heat-treated arc-sprayed coatings might behave like a copper–copper oxide composite material in which ductile deformation by moving dislocation is hindered.

5. Summary and conclusions

In the present study, mechanical properties and micromechanisms of failure modes of cold-sprayed and thermally sprayed copper coatings are investigated for as-sprayed states and different annealing conditions. The results demonstrate that cold-sprayed coatings, which are processed with helium, show a similar performance as highly deformed bulk material. Also after subsequent annealing, strength and elongation to failure develop in a similar manner as for cold rolled sheets. In the as-sprayed state, cold-sprayed coatings, processed with nitrogen, and thermal spray coatings show brittle failure already under comparatively low tensile stress. Whereas the performance of cold-sprayed coatings, processed with nitrogen, can be substantially improved by annealing, mechanical properties of thermal spray coatings are influenced only to a minor extend by following heat treatments. The diffusion during annealing of cold-sprayed coatings can close particle–particle interfaces, which are just under compressive contact and therefore reduce the number of potential crack initiation sites. Heat treatments of thermal spray coatings mainly result in a rearrangement of oxide distributions, which only slightly influences mechanical properties.

With respect to applications, it is of high interest that the performance of cold-sprayed coatings, processed with nitrogen as propellant gas, can be significantly improved by annealing. Annealing procedures at quite moderate temperatures between 400 and 600 °C appear as an economical alternative to the costly use of helium as process gas. Since manufacturing techniques, as for example, soldering, or respective applications can expose coatings to such heat treatments, cold spraying of copper with nitrogen should have a great impact for industrial use. Furthermore, utilizing micro-tensile testing technique for determining the intrinsic mechanical properties of the coatings proved to be a very promising technique for such materials.

Acknowledgements

Significant parts of the research were supported by the Deutsche Forschungsgemeinschaft (DFG), grant number KR 808 1103/3-3, and the Arbeitsgemeinschaft industrieller Forschungsvereinigungen (AiF) grant number 12.671 N, which are greatly acknowledged.

References

[1] H. Kreye, F. Gärtner, H.J. Richter, in: P. Heinrich (Ed.), Proc. 6. Kolloqium Hochgeschwindigkeits – Flammspritzen, Erding, Germany, November 27–28, 2003, Gemeinschaft Thermisches Spritzen e.V., Unterschleißheim, Germany, 2003, p. 5.
[2] F. Gärtner, T. Stoltenhoff, T. Schmidt, H. Kreye, in: E. Lugscheider (Ed.), Thermal Spray Connects: Explore its Surfacing Potential, Proc. Intl. Thermal Spray Conf., May 2–4, 2005, Basel, Switzerland, DVS-Verlag, Düsseldorf, Germany, 2005, p. 158.
[3] R.C. McCune, A.N. Papyrin, J.N. Hall, W.L. Riggs II, P.H. Zajchowski, in: C.C. Berndt, S. Sampath (Eds.), Advances in Thermal Spray Science and Technology, Proc. 8th Nat'l Thermal Spray Conf. ASM International, Materials Park, OH, USA, 1995, p. 1.
[4] T. Stoltenhoff, H. Kreye, H.J. Richter, J. Therm. Spray Technol. 11 (2002) 542.
[5] H. Assadi, F. Gärtner, T. Stoltenhoff, H. Kreye, Acta Mater. 51 (2003) 4379.
[6] T. Stoltenhoff, Kaltgasspritzen von Kupfer – eine strömungsmechanische und werkstoffkundliche Analyse und Optimierung des Spritzprozesses. PhD Thesis, Universität der Bundeswehr Hamburg. Shaker Verlag, Aachen, 2004.
[7] T. Stoltenhoff, C. Borchers, F. Gärtner, H. Kreye, Surf. Coat. Technol. (in press) doi:10.1016/j.surfcoat.2005.05.011.
[8] C. Borchers, F. Gärtner, T. Stoltenhoff, H. Kreye, Acta Mater. 53 (2005) 2991.
[9] D. Grasme, in: P. Heinrich (Ed.), Proc. 6. Kolloqium Hochgeschwindigkeits–Flammspritzen, Erding, Germany, November 27–28, 2003, Gemeinschaft Thermisches Spritzen e.V., Unterschleißheim, Germany, 2003, p. 119.
[10] C.K. Lin, C.C. Berndt, Surf. Coat. Technol. 102 (1998) 1.
[11] G. Burkle, F. Banhart, A. Sagel, C. Wanke, G. Croopnick, H.J. Fecht, Mat. Sci. Forum 386-3 (2002) 571.
[12] J. Voyer, H. Kreye, J. Therm. Spray Technol. 12 (2003) 416.
[13] H. Gassot, T. Junquera, V. Ji, M. Jeandin, V. Guipont, C. Coddet, C. Verdy, L. Grandsire, Surf. Eng. 17 (2001) 317.
[14] E. Calla, D.G. McCartney, P.H. Shipway, in: E. Lugscheider (Ed.), Thermal Spray Connects: Explore its Surfacing Potential, Proc. Intl. Thermal Spray Conf., May 2–4, 2005, Basel, Switzerland, DVS-Verlag, Düsseldorf, Germany, 2005, p. 170.
[15] A.C. Hall, D.J. Cook, R.A. Neiser, T.J. Roemer, D.A. Hirschfeld, in: E. Lugscheider (Ed.), Thermal Spray Connects: Explore its Surfacing Potential, Proc. Intl. Thermal Spray Conf., May 2–4, 2005, Basel, Switzerland, DVS-Verlag, Düsseldorf, Germany, 2005, p. 251.
[16] R.E. Blose, in: E. Lugscheider (Ed.), Thermal Spray Connects: Explore its Surfacing Potential, Proc. Intl. Thermal Spray Conf., May 2–4, 2005, Basel, Switzerland, DVS-Verlag, Düsseldorf, Germany, 2005, p. 199.
[17] M. Kocak, J. dos Santos, S. Riekehr, Sci. Technol. Weld. Join. 6 (2001) 347.
[18] Properties and Selection: Nonferrous Alloys and Special-Purpose Materials, ASM Handbook, vol. 2, ASM International, 1990, pp. 265–345.
[19] C. Borchers, F. Gärtner, T. Stoltenhoff, H. Kreye, H. Assadi, J. Appl. Phys. 93 (2003) 10064.
[20] H. Kreye, in: P. Heinrich (Ed.), Proc. 4. Kolloqium Hochgeschwindigkeits–Flammspritzen, Erding, Germany, November 13–14, 1997, Gemeinschaft Thermisches Spritzen e.V., Unterschleißheim, Germany, 1997, p. 13.
[21] Product information for high purity copper (99.99%): Wieland Werke, Ulm, Germany.